Journal of Materials Chemistry C

ROYAL SOCIETY OF CHEMISTRY

PAPER

View Article Online
View Journal | View Issue



Cite this: J. Mater. Chem. C, 2025, 13, 16954

# Determining interfacial energy levels between the crystalline emitting layer and the amorphous electron transport layer: UPS-assisted efficiency optimization in crystalline OLEDs†

Wenjing Li,[ab] Tianyi Lin,[ab] Feng Zhu *[ab] and Donghang Yan[ab]

In crystalline organic light-emitting diodes (C-OLEDs), the interfacial energy level matching between the amorphous electron transport layer (ETL) and the crystalline emitting layer (EML) is of vital importance for the charge injection efficiency and device performance. In traditional studies, the bulk highest occupied molecular orbital (HOMO)/lowest unoccupied molecular orbital (LUMO) energy levels of a single material are often determined using cyclic voltammetry (CV), and these values are employed to indicate the materials' energy levels in OLEDs. However, this method neglects key factors such as interface energy level bending or offset, which could greatly influence crystalline material interfaces. In this study, taking blue-light 2FPPICz:BPPI C-OLED as the model system and selecting five typical electron transport materials including TmPyPB, TPBI, and Bphen as the amorphous ETL, the key differences in interfacial energy level characterization are revealed through multi-dimensional methods. By comparing the bulk energy levels of the amorphous ETL determined using CV and the interfacial energy levels of the crystalline EML/amorphous ETL measured using ultraviolet photoelectron spectroscopy (UPS), it is found that there is a significant difference between the molecular energy levels measured by CV and the actual interfacial energy levels in C-OLEDs, leading to an obvious deviation between the actual external quantum efficiency (EQE) of the device and the expected value. For example, CV shows that the bulk LUMO and HOMO of Bphen match with that of the EML, but UPS measures an interfacial energy level mismatch, resulting in a maximum external quantum efficiency of only 1.70% for the device, which is much lower than the theoretical expectation. In contrast, although CV shows a large energy difference between the bulk LUMO of TPBI and the EML, UPS measures well-matched interfacial energy levels with only a 0.09 eV energy difference, achieving a high EQE of 5.98%. The research results indicate that interfacial energy level analysis based on UPS can precisely describe the interface physics, guide energy level optimization and improve the luminous efficiency of C-OLEDs. This work proves a necessary characterization paradigm for interface engineering of organic crystalline optoelectronic devices, especially crystalline OLEDs.

Received 3rd May 2025,
Accepted 10th July 2025

DOI: 10.1039/d5tc01782c

rsc.li/materials-c



## Introduction

An organic light-emitting diode (OLED) is the core component of the new generation of display and lighting technologies.[1–3] Its performance always relies on the precise regulation of carrier injection balance, exciton utilization efficiency and exciton recombination efficiency.[4–6] The chemical structure of emitters forms the basis for regulating the above processes. Taking naphthalimide derivatives as an example, their planar conjugated frameworks can precisely tune optoelectronic properties through molecular engineering (such as introducing amino/alkoxy substituents), directly optimizing charge transport efficiency, energy band gaps, and aggregation behavior. Experiments have confirmed that naphthalimide emitters with optimized donor–acceptor configurations can achieve an external quantum efficiency of up to 20.3%, fully verifying the decisive role of molecular design in device performance.[7] In recent years, crystalline organic light-emitting diodes (C-OLEDs) have achieved remarkable results due to high carrier mobility of crystalline organic materials and rational design

[a] State Key Laboratory of Polymer Science and Technology, Changchun Institute of Applied Chemistry, Chinese Academy of Sciences, Changchun 130022, China. E-mail: zhufeng@ciac.ac.cn
[b] School of Applied Chemistry and Engineering, University of Science and Technology of China, Hefei 230026, China

† Electronic supplementary information (ESI) available: Fig. S1–S3. See DOI: https://doi.org/10.1039/d5tc01782c

of device structures.[8–12] However, even when emitters are optimized for excellent intrinsic properties (*e.g.*, high quantum efficiency) through molecular design, the interfacial energy level mismatch with adjacent transport layers (especially the electron transport layer, ETL) may still become a key bottleneck restricting device efficiency. Therefore, exploring how to select amorphous electron transport layers (ETLs) that are compatible with the crystalline emitting layer (EML) is the key to further improving the efficiency of C-OLEDs.

In traditional research, the energy level assessment of ETL materials often relies on cyclic voltammetry (CV),[13] which calculates the highest occupied molecular orbital (HOMO) and lowest unoccupied molecular orbital (LUMO) energy levels of the materials based on their redox potentials.[14] However, such methods can only reflect the bulk phase energy level characteristics of the materials and cannot directly describe the interface energy level arrangement differences between the ETL and EML in the actual working state of the C-OLEDs. This limitation may lead to significant deviations between theoretical design and actual device performance, such as unpredictable interface charge injection barriers or intensified exciton quenching effects, ultimately restricting the improvement of device efficiency and lifetime.[15]

Ultraviolet photoelectron spectroscopy (UPS)[16] technology provides more reliable experimental evidence for revealing the interface energy level relationships in real devices due to its ability to directly measure the work function, and band bending characteristics of materials in the film state.[17,18] However, the energy level selection criteria and interface engineering for ETL materials in C-OLEDs still widely rely on CV data in the bulk phase, and the practical interfacial physical image obtained *via* UPS has not been systematically explored.

This study uses typical blue light 2-(4-(9*H*-carbazol-9-yl)-phenyl)-1-(3,5-difluorophenyl)-1*H*-phenanthro[9,10-*d*]imidazole (2FPPICz):4,4′-bis-)1-phenyl-phenanthro[9,10-*d*]imidazol-2-yl)-biphenyl (BPPI) C-OLEDs[8] as a model system. By comparing the bulk phase energy levels (*via* CV) and interface energy levels (*via* UPS) of five ETL materials (1,3,5-tri[(3 -pyridyl)-phen-3-yl]benzene (TmPyPB),[19] 1,3,5-tri(1-phenyl-1*H*-benzo-[*d*]imidazol-2-yl)phenyl (TPBI),[20] *etc.*), we reveal the limitations of the traditional CV method in ETL energy level assessment. Experiments show that the correlation between the ΔLUMO (LUMO energy level difference between EML and ETL interfaces) obtained based on UPS and the C-OLED efficiency is significantly better than that predicted using the CV method. For example, although the CV method shows that the bulk phase LUMO of 4,7-diphenyl-1,10-phenanthroline (Bphen)[21] matches well with the EML, the interface energy level mismatch exposed by UPS testing directly leads to a very low device efficiency, of which the maximum external quantum efficiency ($EQE_{max}$) = 1.70%. This discovery not only challenges the traditional energy level selection paradigm but also emphasizes the core position of interface energy level engineering in the design of C-OLEDs. This work provides new methodological guidance for the optimization of transport layers in high-performance C-OLEDs.

## Results and discussion

### Energy level characterization of interfaces between the crystalline EML and amorphous ETLs

In order to select the most suitable scheme for choosing ETLs for C-OLEDs, we need to compare the material energy level data obtained through the CV and UPS testing methods. Based on a 2FPPICz:BPPI thin film as the crystalline EML of C-OLED,[8] we selected five electron transport materials including TPBI, TmPyPB, 1,3-bis[3,5-di(pyridin-3-yl)phenyl]benzene(BmPyPhB),[22] bis[2-(2-hydroxyphenyl)-pyridine]beryllium ($Be(pp)_2$)[23] and Bphen for the study. Fig. S1 (ESI†) shows the LUMO and HOMO data of these five materials obtained from CV measurements, all from the ref. 21, 24 and 25.

Fig. 1 shows the UV-vis absorption spectra of 2FPPICz:BPPI crystalline thin film and five electron transport layers (ETLs). The absorption edge wavelength of 2FPPICz:BPPI, BmPyPhB, TPBI, TmPyPB, $Be(pp)_2$ and Bphen are 384 nm, 311 nm, 352 nm, 307 nm, 406 nm and 405 nm, respectively. Meanwhile, the UV-vis absorption spectrum of the amorphous 2FPPICz:BPPI thin film was also measured and is presented in Fig. S2 (ESI†). Consistent with previously reported findings, the ordered molecular arrangement in the crystalline thin film leads to distinct energy levels and excited state distributions between the crystalline and amorphous phases. This difference causes the absorption edge (399 nm) of the amorphous thin film to exhibit a certain degree of red-shift compared to that of the crystalline thin film.[26,27] According to formula (1),[28] the optical bandgap ($E_g$) can be estimated.

$$E_g\,(\mathrm{eV}) = h \times \frac{c}{\lambda} \approx \frac{1240}{\lambda} \qquad (1)$$

$\lambda$ is the absorption edge wavelength of the film. Table 1 presents the $E_g$ values of the crystalline emitting layer (EML) of 2FPPICz:BPPI and five amorphous ETLs calculated based on the absorption band edges. The calculated $E_g$ values of the 2FPPICz:BPPI crystalline thin film, BmPyPhB, TPBI, TmPyPB,

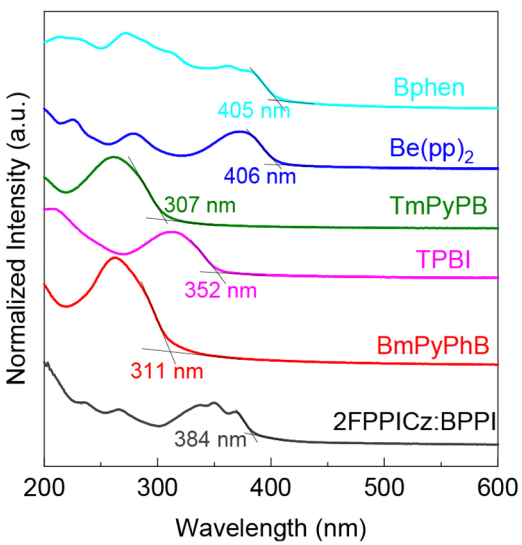


Fig. 1 UV-vis absorption spectra of the 2FPPICz:BPPI crystalline thin film and BmPyPhB, TPBI, TmPyPB, $Be(pp)_2$ and Bphen amorphous thin films.

Table 1 Bandgap energy ($E_g$) of the 2FPPICz:BPPI crystalline thin film and the amorphous thin film of BmPyPhB, TPBI, TmPyPB, $Be(pp)_2$ and Bphen, which were determined using the UV-Visible absorption spectra shown in Fig. 1

| Material | $E_g$ (eV) |
|---|---|
| 2FPPICz:BPPI | 3.23 |
| TPBI | 3.52 |
| BmPyPhB | 3.99 |
| TmPyPB | 4.04 |
| $Be(pp)_2$ | 3.05 |
| Bphen | 3.06 |

$Be(pp)_2$ and Bphen amorphous thin films are 3.23 eV, 3.99 eV, 3.52 eV, 4.04 eV, 3.05 eV and 3.06 eV, respectively. The observed $E_g$ variations (3.05–4.04 eV) are primarily governed by molecular planarity and substituent effects. Planar metal complexes like $Be(pp)_2$ and Bphen exhibit the narrowest $E_g$ due to their fully conjugated rigid backbones, enabling efficient π-electron delocalization.[29,30] The 2FPPICz:BPPI blend shows an intermediate $E_g$ of 3.23 eV, attributed to intermolecular charge transfer between the electron-donating 2FPPICz and electron-accepting BPPI, which stabilizes the excited state and lowers the energy barrier.[31] In contrast, twisted aromatic materials such as TPBI, BmPyPhB and TmPyPB display wider $E_g$ values (3.52–4.04 eV) due to structural non-planarity induced by bulky substituents, which disrupts π-conjugation and reduces orbital overlap.

We fabricated the following structure of thin films for UPS testing. Indium tin oxide(ITO)/poly(3,4-ethylenedioxythiophene): poly(styrenesulfonate) (PEDOT:PSS)/2,5-di([1,1′-biphenyl]-4-yl)-thiophene (BP1T) (7 nm)/2FPPICz (10 nm)/2FPPICz:BPPI

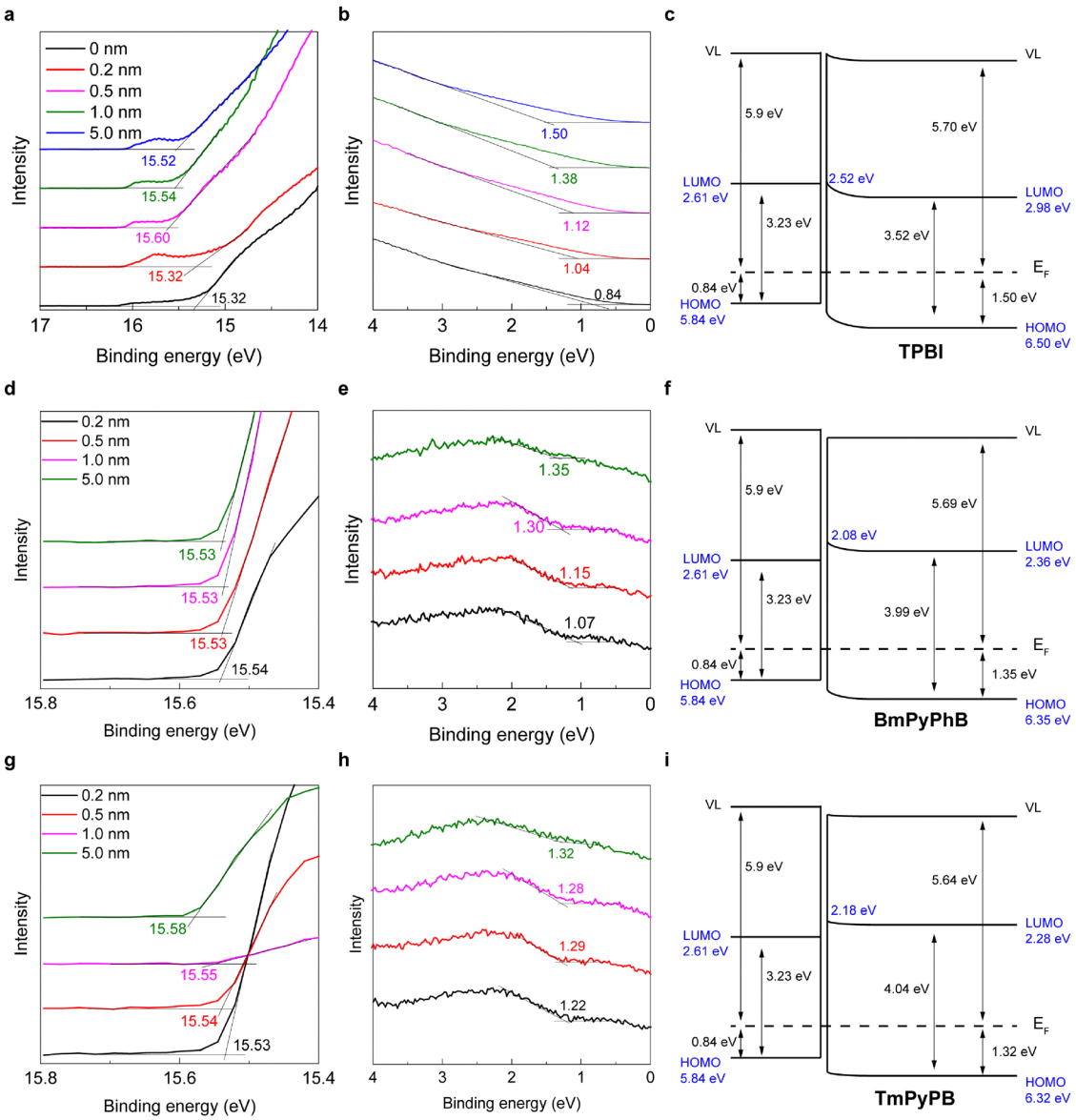


Fig. 2 UPS characterization and schematic energy level diagram of the 2FPPICz:BPPI crystalline film and ETL organic heterojunction (a)–(c) TPBI (d)–(f) BmPyPhB (g)–(i) TmPyPB.

 

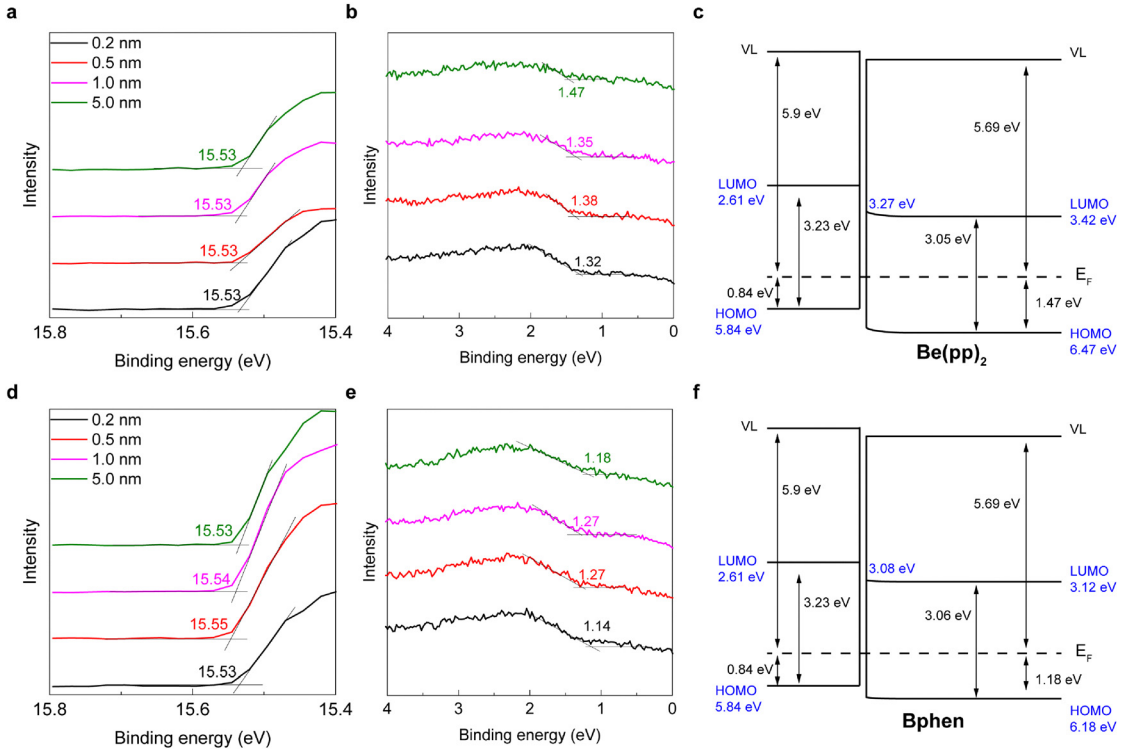


Fig. 3 UPS characterization and schematic energy level diagram of the 2FPPICz:BPPI crystalline film and ETL organic heterojunction (a)–(c) $Be(pp)_2$ (d)–(f) Bphen.

(6% 20 nm) and ITO/PEDOT:PSS/BP1T (7 nm)/2FPPICz (10 nm)/2FPPICz:BPPI (6% 20 nm)/ETLs (0.2 nm, 0.5 nm, 1 nm, 5 nm). ETLs consist of BmPyPhB, TPBI, TmPyPB, $Be(pp)_2$ and Bphen these five materials. Fig. 2 and 3 show the UPS characterization and schematic energy level diagrams of 2FPPICz:BPPI crystalline thin film and ETLs (BmPyPhB, TPBI, TmPyPB, $Be(pp)_2$ and Bphen) organic heterojunction. "0 nm" curve of Fig. 2a shows the high binding energy cut-off (HBEC) of the 2FPPICz:BPPI crystalline thin film. "0 nm" curve of Fig. 2b represents the HOMO of 2FPPICz:BPPI crystalline thin film. Based on the work function of the reference electrode Au being 5.0 eV in the test, combined with the $E_g$ value of the 2FPPICz:BPPI crystalline film being 3.23 eV, it can be concluded that the HOMO and the LUMO of 2FPPICz:BPPI crystalline thin film is 5.84 eV and 2.61 eV, respectively. Among them, as the thickness of the amorphous films of TPBI and TmPyPB increases, the position of HBEC shifts towards higher energy. This indicates that the vacuum energy level (VL) of the interface between the crystalline film of 2FPPICz:BPPI and these two ETL amorphous films has shifted. The HBEC of other three ETLs do not shift with the increase of thickness, indicating that their vacuum energy levels have not shifted. As the thickness of ETLs increases, the HOMO of the five ETLs all show a shift towards higher energy. This indicates that the HOMO energy levels of ETLs bend downward from the interface to the bulk phase, *i.e.* interfacial heterojunction effect exists. HOMO of TPBI, BmPyPhB, TmPyPB, $Be(pp)_2$ and Bphen (bulk phase) are 6.50 eV, 6.35 eV, 6.32 eV, 6.47 eV and 6.18 eV, respectively. Based on the $E_g$ values of the five ETLs, their LUMOs were calculated. The LUMO (bulk phase) of TPBI, BmPyPhB, TmPyPB, $Be(pp)_2$ and Bphen are 2.98 eV, 2.36 eV, 2.28 eV, 3.42 eV and 3.12 eV, respectively. Based on the HOMO information of 0.2 nm thickness ETLs, we obtained the LUMO of five kinds of ETLs at the interface. Among them, LUMOs (at 0.2 nm) of TPBI, BmPyPhB, TmPyPB, $Be(pp)_2$ and Bphen are 2.52 eV, 2.08 eV, 2.18 eV, 3.27 eV and 3.08 eV, respectively. Therefore, by comparing the two sets of results, we can conclude that the results obtained from the CV test alone can only represent the energy level information of the material itself. As for the actual energy level arrangement of the interface contact, it needs to be determined *via* the UPS test method.

### Fabrication and characterization of C-OLEDs

The energy level matching between the light-emitting layer and the electron transport layer is of great significance for the performance of C-OLEDs. In the previous chapter, through UPS testing, we obtained the actual energy level arrangement of the interface between the EML and the ETLs. Next, we fabricate C-OLEDs based on these five ETLs and explore the correlation between the interfacial energy levels and the device performance. We fabricated C-OLEDs with the following structure:

ITO/PEDOT:PSS/BP1T(7 nm)/2FPPICz(10 nm)/2FPPICz:BPPI (20 nm 6%)/ETLs (40 nm)/LiF (1 nm)/Al (120 nm). Crystalline thin films are fabricated through the WEG method.[27,32–34] BP1T is the inducing layer of the crystalline thin film.[35] 2FPPICz is the crystalline hole transport layer (HTL), and 2FPPICz:BPPI is

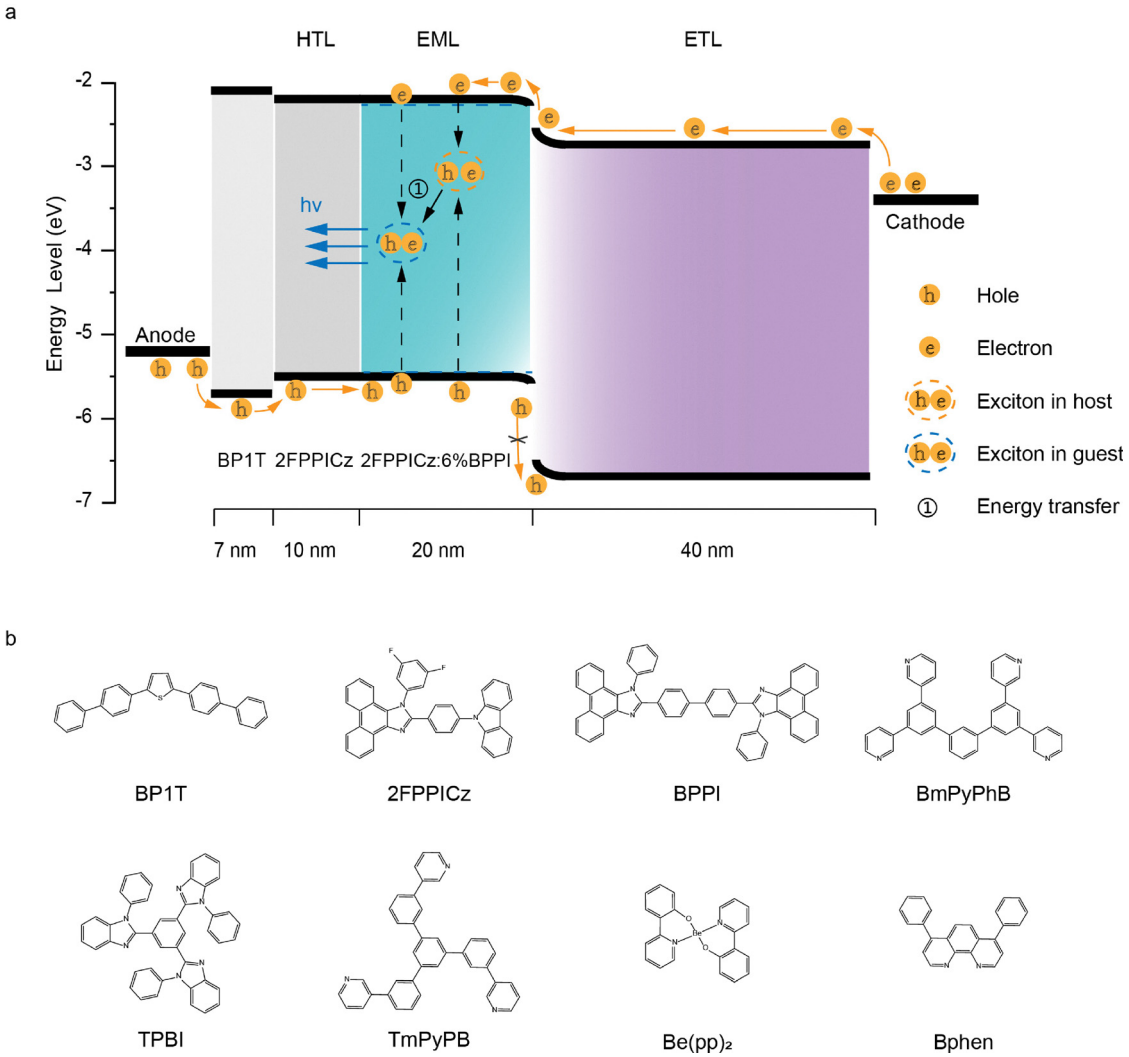


Fig. 4 Device structure of the solid-solution C-OLED. (a) Schematic illustration of the device structure consisting of the induced layer (BP1T), WEG layer (2FPPICz), crystalline organic solid-solution thin films and electron transport layer. (b) Structural formulas of the emissive layer host material 2FPPICz, guest material BPPI and five electron transport materials used in this article.

the crystalline emitting layer (EML). The inducing layer, HTL and EML were all deposited at a base temperature of 102 °C. According to previous studies,[8] the crystalline light-emitting layer 2FPPICz:BPPI is a crystalline organic solid solution (non-stoichiometric multicomponent crystal) thin film, in which 2FPPICz and BPPI are co-doped at different mass ratios. The pure 2FPPICz thin film exhibits smooth strip-like crystals, and BPPI molecules are doped into the crystalline framework of the host 2FPPICz *via* a substitutional mechanism. Notably, the incorporation of BPPI molecules does not disrupt the crystalline framework of the 2FPPICz thin film. The ETLs TPBI, BmPyPhB, TmPyPB, $Be(pp)_2$ and Bphen amorphous thin films were deposited at a base room-temperature. Fig. 4a presents the schematic diagram of the principle of C-OLEDs. The device consists of three simple parts, namely HTL, EML and ETL. A bias voltage is applied between the cathode Al and the anode ITO. Holes and electrons are respectively injected into the EML from the anode and the cathode, forming excitons and generating light emission. Fig. 4b presents the chemical formulas of all the materials used in this paper.

Fig. 5 depicts the device performance of C-OLEDs using different ETLs. Fig. 5a shows the current density ($J$)–voltage ($V$)–luminance ($L$) curve. Fig. 5b presents the electroluminescence (EL) spectra. All the C-OLEDs fabricated with the five ETLs emit blue light with a peak around 450 nm. Fig. 5c presents the curves of current efficiency (CE) and luminance. Among them, the maximum current efficiencies ($CE_{max}$) of TmPyPB, TPBI, BmPyPhB, $Be(pp)_2$ and Bphen are 5.50 cd $A^{-1}$, 5.12 cd $A^{-1}$, 4.66 cd $A^{-1}$, 3.20 cd $A^{-1}$ and 1.93 cd $A^{-1}$, respectively. Fig. S2 (ESI†) presents the curves of power efficiency (PE) and luminance. Among them, the maximum power efficiency ($PE_{max}$) of TmPyPB, TPBI, BmPyPhB, $Be(pp)_2$ and Bphen are 5.42 lm $W^{-1}$, 5.15 lm $W^{-1}$, 4.57 lm $W^{-1}$, 3.25 lm $W^{-1}$ and 2.02 lm $W^{-1}$, respectively. Fig. 5d presents the curves of external quantum efficiency (EQE) *vs.* luminance. Among them, the $EQE_{max}$ of TPBI, BmPyPhB, TmPyPB, $Be(pp)_2$ and Bphen from

 

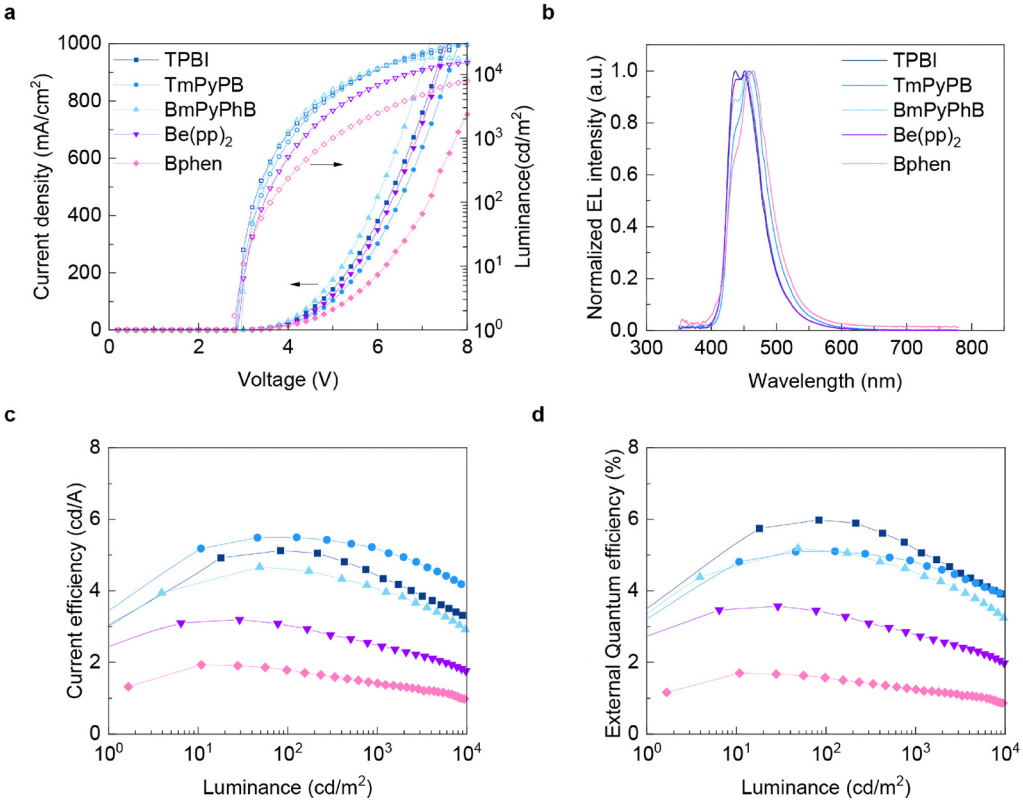


Fig. 5 Device performance of C-OLEDs using different ETLs (a) current density–voltage–luminance and (b) EL spectrum (c) current efficiency curves and (d) external quantum efficiency curves of C-OLEDs.

the largest to the smallest are 5.98%, 5.19%, 5.10%, 3.57% and 1.70%, respectively.

Based on UPS test results and the performance results of C-OLEDs, we conducted an analysis. In Fig. 6, the relationship between the ETL thickness and the LUMO and HOMO is presented, as well as the relationship between ΔLUMO (the difference in LUMO energy levels between the EML and the ETLs at the interface) and the current efficiency (left) and external quantum efficiency (right) of C-OLEDs at 100 cd $m^{-2}$ and 1000 cd $m^{-2}$ luminance levels are shown respectively. Fig. 6a demonstrates that, starting from the EML interface of 2FPPICz:BPPI (0 nm thickness), the LUMO energy levels of the five electron transport layers exhibit variations with increasing ETL thickness. At 0.2 nm thickness, the LUMO energy levels of BmPyPhB, TmPyPB and TPBI are higher than the LUMO of the 2FPPICz:BPPI crystalline surface. Among them, the interface potential barriers ΔLUMO (ΔLUMO = LUMO(EML) − LUMO(ETL)) of BmPyPhB, TmPyPB and TPBI are −0.53 eV, −0.43 eV and −0.09 eV respectively. The $EQE_{max}$ of C-OLEDs fabricated using BmPyPhB, TmPyPB and TPBI are 5.19%, 5.10% and 5.98% respectively. At 0.2 nm, the LUMO of the interface of $Be(pp)_2$ and Bphen materials is lower than that of the EML in the crystalline state, and the ΔLUMO values are 0.66 eV and 0.47 eV respectively. The $EQE_{max}$ of C-OLEDs fabricated using $Be(pp)_2$ and Bphen are 3.57% and 1.70%, respectively. It can be seen that when the LUMO of ETL at the interface is higher than that of the crystalline EML, it is beneficial for C-OLED to achieve a higher external quantum efficiency. Fig. 6b illustrates the changes in the HOMO positions of the five kinds of ETLs as their thicknesses increase. When the ETL thickness is 5 nm, the bulk phase HOMOs of TPBI, TmPyPB, BmPyPhB, $Be(pp)_2$ and Bphen are 6.50 eV, 6.32 eV, 6.35 eV, 6.47 eV and 6.18 eV respectively. Since the absolute value of the difference between the HOMO of Bphen and the HOMO of the EML is the smallest, the $EQE_{max}$ of the C-OLED with Bphen ETL is the lowest, reaching 1.70%. Fig. 6c and d illustrate the ΔLUMO dependence of the current efficiency (left) and external quantum efficiency (right) of C-OLEDs at the luminance levels of 100 cd $m^{-2}$ (Fig. 6c) and 1000 cd $m^{-2}$ (Fig. 6d). Summarizing the information we had obtained previously, the LUMO data in Fig. 6a and d were obtained through UPS testing. LUMO data in Fig. 6e and f were derived from Fig. S1 (ESI†) and measured using the CV method. It can be observed that the relationship between the performance of the C-OLED and the LUMO energy level (the CV method) is irregular. Therefore, when regulating the performance of C-OLED, using only the CV method to determine the energy level matching is inaccurate.

## Conclusions

In conclusion, this study systematically analyzed the energy level selection strategy of the ETL in C-OLEDs, revealing the

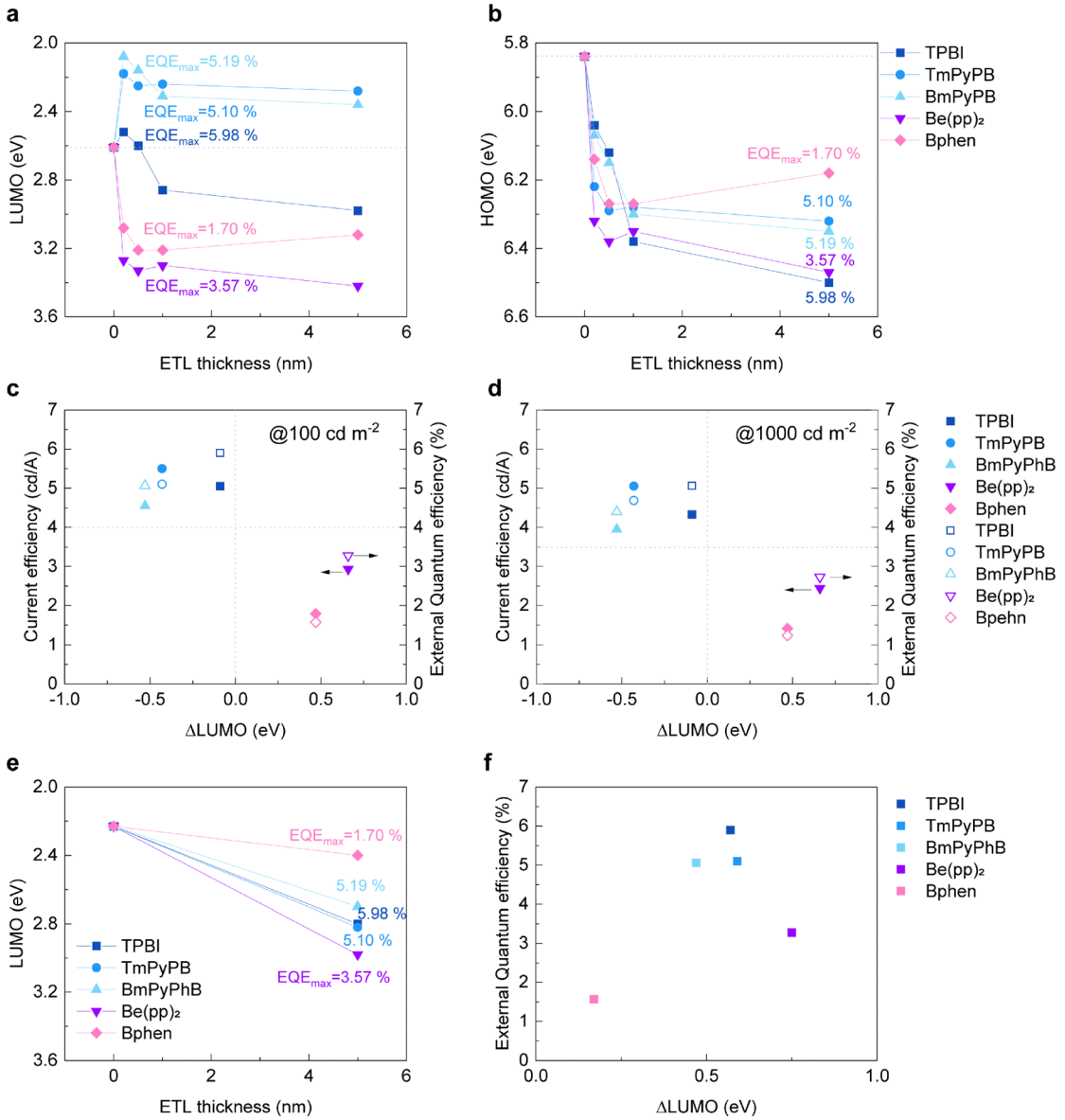


Fig. 6 The relationship between the ETL thickness and (a) LUMO and (b) HOMO. The relationship between ΔLUMO (the energy level difference between EML and ETLs) and current efficiency and external quantum efficiency @ (c) 100cd m$^{-2}$ (d) 1000cd m$^{-2}$. LUMOs of (a)–(d) were measured using UPS. (e) The relationship between the ETL thickness and LUMO, (f) relationship between ΔLUMO and EQE$_{max}$. The LUMO of (e) and (f) were measured by CV, data from ref. 21, 24, 25, 34 and 36.

limitations of the traditional CV method in evaluating the interface energy levels of crystalline EML and amorphous ETL. An important paradigm for interface energy level characterization based on UPS was proposed and proved. Experiments demonstrated that there was a significant deviation between the bulk LUMO energy level of the ETL material as determined by CV (*e.g.*, 2.8 eV for TPBI, 2.7 eV for BmPyPB, 2.82 eV for TmPyPB, 2.98 eV for Be(pp)$_2$, 2.4 eV for Bphen) and the interface LUMO energy level as characterized using UPS (*e.g.*, 2.52 eV for TPBI, 2.08 eV for BmPyPB, 2.18 eV for TmPyPB, 3.27 eV for Be(pp)$_2$, 3.08 eV for Bphen), representing ~0.28 eV, 0.62 eV, 0.64 eV, 0.29 eV, 0.68 eV difference for TPBI, BmPyPB, TmPyPB, Be(pp)$_2$, Bphen. Therefore, relying solely on CV data for designing the ETL would lead to serious interface energy level mismatch. UPS provides atomic-level accuracy as an experimental basis for interface engineering and is a core tool for optimizing charge injection efficiency. When the LUMO energy levels of the crystalline EML/amorphous ETL interface match (TPBI, TmPyPB, and BmPyPhB), the electron injection efficiency is high, achieving a high EQE (*e.g.*, 5.98% for TPBI, 5.10% for TmPyPB, 5.19% for BmPyPB); conversely, Be(pp)$_2$ and Bphen would lead to electron injection obstruction and a decrease in device efficiency (*e.g.*, 3.57% for Be(pp)$_2$, 1.70% for Bphen). Moreover, from the relationship between ETL thickness (0.2–5.0 nm) and interface energy level offset, the interfacial heterojunction effect of ultra-thin ETL cannot be ignored and its energy level physical image needs to be guided by UPS.

# Method

### Materials

The organic semiconductor materials 2-(4-(9*H*-carbazol-9-yl)phenyl)-1-(3,5-difluorophenyl)-1*H*-phenanthro[9,10-*d*]imidazole (2FPPICz) were purchased from Jilin Yuanhe Electronic Material Company. Before use, it was purified twice by thermal gradient sublimation. Poly(3,4-ethylenedioxythiophene):poly(styrenesulfonate) (PEDOT:PSS Clevious PVP Al4083) was purchased from Heraeus. BmPyPhB and BPPI were purchased from Luminescence technology corporation (Lumtec). TPBI, TmPyPB, Bphen, $Be(pp)_2$ and LiF were all purchased from Jilin OLED material Tech Co. Ltd; these materials were not additional purified before use.

### Film and device fabrication

Using indium tin oxide(ITO)-patterned glass substrates (thickness of 180 nm and sheet resistance of 10 Ω per square) to fabricate OLEDs. As a pretreatment for deposition, ITO substrates were thoroughly cleaned sequentially with cleanser, acetone, methanol and deionized water in an ultrasonic bath. This was followed by a 30 minutes' drying period at 120 °C. After cleaning, ITO substrates were treated with oxygen plasma. After spin coating at 600 rpm for 6 seconds, PEDOT:PSS was then spin coated at 4000 rpm for 30 seconds, and finally baked at 120 °C for 30 minutes.

The organic semiconductor device was fabricated *via* physical vacuum deposition. ITO substrates were then transferred to a vacuum evaporation device chamber for device evaporation at a vacuum of $10^{-4}$ after the above treatment. Organic crystalline films are BP1T, 2FPPICz, and 2FPPICz:BPPI. A BP1T layer is an induced layer, while a 2FPPICz pure layer is an epitaxial crystalline layer. 2FPPICz:BPPI (6%) is the OSS EML. The preparation of BP1T,2FPPICz and 2FPPICz:BPPI layer adopts a similar WEG method reported previously.[32] All of the ETLs used in this article are amorphous thin films. The substrate temperatures for fabricating crystalline organic and amorphous thin films are 102 °C and room temperature, respectively. When evaporating organic layer and LiF, the substrate rotation speed is 450 r.p.m. The deposition rates of BP1T and 2FPPICz are about 4–10 Å $min^{-1}$. The deposition rates of the 2FPPICz:BPPI layer of 2FPPICz and BPPI are 10 Å $min^{-1}$ and 0.2–1.0 Å $min^{-1}$ respectively. The deposition rates of BmPyPhB, TPBI, TmPyPB, $Be(pp)_2$ and Bphen are 1–2 Å $s^{-1}$ at room temperature. The deposition rate of LiF and Al are 3–5 Å $min^{-1}$ and 10–15 Å $s^{-1}$ at room temperature, respectively. A quartz-crystal microbalance was used for monitoring the film thickness. The area of device emission is determined by the intersection between the anode (ITO) and cathode (Al) (that is 4 mm × 4 mm).

### Thin film and device characterization

The thickness of films were measured using a RIGAKU Smartlab X-ray diffractometer (Cu Kα $\lambda$ = 1.54056 Å) with the out-of-plane mode. A Shimadzu UV-3600 spectrometer was used to measure the ultraviolet-visible absorption spectra. UPS was conducted by sending samples to the company ZHONGKE E TEST for testing. The current density–voltage–luminance (*J*–*V*–*L*) characteristics were measured using a Keithley 2400/2000 source-measure unit with a calibrated silicon photodiode, and the electroluminescence (EL) spectra were measured using a SpectraScan PR650 spectrophotometer under an ambient laboratory atmosphere at room temperature. By assuming a Lambertian distribution, the EQE was obtained from the current density, luminance and electroluminescence spectra.

# Author contributions

F. Z. and D. Y. initiated and designed the research. W. L. carried out the growth of thin films, the fabrication and characterization of OLEDs. T. L. assisted in conducting sample preparation and tests for UPS experiments. F. Z. and D. Y. supervised the project. All authors discussed the results, prepared and commented on the manuscript.

# Conflicts of interest

The authors declare that they have no competing interests.

# Data availability

All data are available in the main text or the ESI.†

# Acknowledgements

This work was funded by the National Key R&D Program of China (Grant No. 2023YFB3608800 to F. Z.) and the National Natural Science Foundation of China (Grant No. 52373198 to F. Z.).

# References

1 K. T. Kamtekar, A. P. Monkman and M. R. Bryce, Recent Advances in White Organic Light-Emitting Materials and Devices (WOLEDs), *Adv. Mater.*, 2010, **22**, 572–582, DOI: **10.1002/adma.200902148**.
2 M. Zhu and C. Yang, Blue fluorescent emitters: design tactics and applications in organic light-emitting diodes, *Chem. Soc. Rev.*, 2013, **42**, 4963–4976, DOI: **10.1039/C3CS35440G**.
3 J.-Y. Hu, *et al.*, Bisanthracene-Based Donor–Acceptor-type Light-Emitting Dopants: Highly Efficient Deep-Blue Emission in Organic Light-Emitting Devices, *Adv. Funct. Mater.*, 2014, **24**, 2064–2071, DOI: **10.1002/adfm.201302907**.
4 X. Qiao, *et al.*, Controlling charge balance and exciton recombination by bipolar host in single-layer organic light-emitting diodes, *J. Appl. Phys.*, 2010, **108**, 034508, DOI: **10.1063/1.3457672**.
5 R. Meerheim, *et al.*, Influence of charge balance and exciton distribution on efficiency and lifetime of phosphorescent organic light-emitting devices, *J. Appl. Phys.*, 2008, **104**, 014510, DOI: **10.1063/1.2951960**.
6 G.-D. Ye, *et al.*, Unveiling the Interfacial Properties of Organic Single-Crystal Hole-Transporting Layers for High-Performance Light-Emitting Devices, *SmartMat*, 2025, **6**, e1329, DOI: **10.1002/smm2.1329**.

7 M. Hosseinnezhad, S. Nasiri, V. Nutalapati, K. Gharanjig and A. M. Arabi, A Review of the Application of Organic Dyes Based on Naphthalimide in Optical and Electrical Devices, *Prog. Color, Color. Coat.*, 2024, **17**, 417–433.
8 P. Sun, D. Liu, F. Zhu and D. Yan, An efficient solid-solution crystalline organic light-emitting diode with deep-blue emission, *Nat. Photonics*, 2023, **17**, 264–272, DOI: **10.1038/s41566-022-01138-0**.
9 Y. Liu, F. Zhu, Y. Wang and D. Yan, High-efficiency crystalline white organic light-emitting diodes, *Light:Sci. Appl.*, 2024, **13**, 86, DOI: **10.1038/s41377-024-01428-y**.
10 J. Yang, D. Hu, F. Zhu, Y. Ma and D. Yan, High-efficiency blue-emission crystalline organic light-emitting diodes sensitized by ''hot exciton'' fluorescent nanoaggregates, *Sci. Adv.*, 2022, **8**(50), eadd1757, DOI: **10.1126/sciadv.add1757**.
11 W. Zheng, F. Zhu and D. Yan, High-Efficiency and Low Efficiency Roll-Off Blue-Emission Crystalline Organic Light-Emitting Diodes by embedding Triplet-Triplet Annihilation Nanoaggregates, *Adv. Opt. Mater.*, 2025, **13**, 2402335, DOI: **10.1002/adom.202402335**.
12 S. Zou, *et al.*, Bipolar Solid-Solution Hosts for Efficient Crystalline Organic Light-Emitting Diodes, *ACS Appl. Mater. Interfaces*, 2025, **17**, 8084–8094, DOI: **10.1021/acsami.4c20265**.
13 L. Leonat, G. Sbrcea and I. V. Branzoi, Cyclic voltammetry for energy levels estimation of organic materials, *Sci. Bull. – Politeh. Univ. Bucharest, Ser. B*, 2013, **75**, 111–118.
14 B.-G. Kim, *et al.*, Energy Level Modulation of HOMO, LUMO, and Band-Gap in Conjugated Polymers for Organic Photovoltaic Applications, *Adv. Funct. Mater.*, 2013, **23**, 439–445, DOI: **10.1002/adfm.201201385**.
15 C. Murawski, K. Leo and M. C. Gather, Efficiency Roll-Off in Organic Light-Emitting Diodes, *Adv. Mater.*, 2013, **25**, 6801–6827, DOI: **10.1002/adma.201301603**.
16 X. M. Ding, *et al.*, Modification of the hole injection barrier in organic light-emitting devices studied by ultraviolet photoelectron spectroscopy, *Appl. Phys. Lett.*, 2000, **76**, 2704–2706, DOI: **10.1063/1.126449**.
17 M. B. Casu, P. Imperia, S. Schrader and B. Falk, Ultraviolet photoelectron spectroscopy of thin films of new materials for multilayer organic light emitting diodes, *Surf. Sci.*, 2001, **482–485**, 1205–1209, DOI: **10.1016/S0039-6028(01)00733-6**.
18 S. M. Tadayyon, *et al.*, CuPc buffer layer role in OLED performance: a study of the interfacial band energies, *Org. Electron.*, 2004, **5**, 157–166, DOI: **10.1016/j.orgel.2003.10.001**.
19 S.-J. Su, T. Chiba, T. Takeda and J. Kido, Pyridine-Containing Triphenylbenzene Derivatives with High Electron Mobility for Highly Efficient Phosphorescent OLEDs, *Adv. Mater.*, 2008, **20**, 2125–2130, DOI: **10.1002/adma.200701730**.
20 J. Calimano, *et al.*, Solid-State Properties and Spectroscopic Analysis of Thin-Film TPBi, *J. Phys. Chem. C*, 2020, **124**, 23716–23723, DOI: **10.1021/acs.jpcc.0c06959**.
21 D. Y. Kondakov, Voltammetric study of Bphen electron-transport layer in contact with LiF/Al cathode in organic light-emitting diodes, *J. Appl. Phys.*, 2006, **99**, 024901, DOI: **10.1063/1.2159549**.
22 P. Chen, *et al.*, Efficient white organic light-emitting diodes with double co-host emitting layers, *J. Mater. Chem. C*, 2018, **6**, 9890–9896, DOI: **10.1039/C8TC03566K**.
23 Y. Wang, Y. Dai and D. Ma, Electron Transport Characteristics in Bepp2:Liq Thin Film and Its Influence on Electroluminescent Device Performance, *J. Phys. Chem. C*, 2020, **124**, 7661–7667, DOI: **10.1021/acs.jpcc.9b11995**.
24 B. S. Kim and J. Y. Lee, Engineering of Mixed Host for High External Quantum Efficiency above 25% in Green Thermally Activated Delayed Fluorescence Device, *Adv. Funct. Mater.*, 2014, **24**, 3970–3977, DOI: **10.1002/adfm.201303730**.
25 Y.-M. Wang, *et al.*, Investigating energy level alignments at organic–organic interfaces in practical devices, *Appl. Phys. Lett.*, 2024, **125**(6), 061603, DOI: **10.1063/5.0220291**.
26 D. Liu, F. Zhu and D. Yan, Crystalline organic thin films for crystalline OLEDs (II): weak epitaxy growth of phenanthroimidazole derivatives, *RSC Adv.*, 2023, **13**, 15586–15593, DOI: **10.1039/D3RA03095D**.
27 J. Xin, P. Sun, F. Zhu, Y. Wang and D. Yan, Doped crystalline thin-film deep-blue organic light-emitting diodes, *J. Mater. Chem. C*, 2021, **9**, 2236–2242, DOI: **10.1039/D0TC05934J**.
28 J. C. S. Costa, R. J. S. Taveira, C. F. R. A. C. Lima, A. Mendes and L. M. N. B. F. Santos, Optical band gaps of organic semiconductor materials, *Opt. Mater.*, 2016, **58**, 51–60, DOI: **10.1016/j.optmat.2016.03.041**.
29 Y. Che and D. F. Perepichka, Quantifying Planarity in the Design of Organic Electronic Materials, *Angew. Chem., Int. Ed.*, 2021, **60**, 1364–1373, DOI: **10.1002/anie.202011521**.
30 T. Haciefendioglu and E. Yildirim, The role of donor units in band gap engineering of donor–acceptor conjugated polymers, *J. Mol. Graph. Model.*, 2025, **138**, 109033, DOI: **10.1016/j.jmgm.2025.109033**.
31 H. Yao, *et al.*, Design, Synthesis, and Photovoltaic Characterization of a Small Molecular Acceptor with an Ultra-Narrow Band Gap, *Angew. Chem., Int. Ed.*, 2017, **56**, 3045–3049, DOI: **10.1002/anie.201610944**.
32 H. Wang, F. Zhu, J. Yang, Y. Geng and D. Yan, Weak Epitaxy Growth Affording High-Mobility Thin Films of Disk-Like Organic Semiconductors, *Adv. Mater.*, 2007, **19**, 2168–2171, DOI: **10.1002/adma.200602566**.
33 J. Yang and D. Yan, Weak epitaxy growth of organic semiconductor thin films, *Chem. Soc. Rev.*, 2009, **38**, 2634–2645, DOI: **10.1039/B815723P**.
34 J. Xin, *et al.*, High-efficiency non-doped deep-blue fluorescent organic light-emitting diodes based on carbazole/phenanthroimidazole derivatives, *J. Mater. Chem. C*, 2020, **8**, 10185–10190, DOI: **10.1039/D0TC02594A**.
35 L. Liu, *et al.*, Highly oriented crystalline thin film with high electroluminescence performance fabricated by weak epitaxy growth, *Org. Electron.*, 2020, **84**, 105806, DOI: **10.1016/j.orgel.2020.105806**.
36 Z. Wang, *et al.*, Phenanthro[9,10-d]imidazole as a new building block for blue light emitting materials, *J. Mater. Chem.*, 2011, **21**, 5451–5456, DOI: **10.1039/C1JM10321K**.

 